Long-Term *RXTE* Monitoring of Anomalous X-ray Pulsars

Fotis P. Gavriil[1] , Victoria M. Kaspi [1,2,3]

ABSTRACT

We report on long-term monitoring of three anomalous X-ray pulsars using the *Rossi X-ray Timing Explorer* (*RXTE*). We present a phase-coherent timing ephemeris for 4U 0142+61, and show that it has rotated with high stability over 4.4 yr, with RMS phase deviations of 7% of the pulse period from a simple fit including only ν and $\dot{\nu}$. We report on the continued timing stability of 1E 2259.1+586, for which phase coherence has now been maintained over 4.5 yr, as well as on the detection of a significant $\ddot{\nu}$ in 1.4 yr of monitoring of RXS J170849.0–400910, consistent with recovery following a glitch. We note a correlation in which timing stability in AXPs decreases with increasing $\dot{\nu}$. The timing stability of soft gamma repeaters in quiescence is consistent with this trend, given their large spin-down rates. This trend is similar to one seen in radio pulsars, suggesting a connection between the three populations. We find no large variability in pulse morphology as a function of time. We present high signal-to-noise ratio average pulse profiles for each AXP, and consider them as a function of energy. We find a variety of different behaviors, and consider possible trends in the data. We also find no large variations in pulsed flux, and set 1σ upper limits of $\sim$20–30% of the mean.

Subject headings: pulsars: general — pulsars: individual (4U 0142+61, RXS J170849.0–400910, 1E 2259.1+586) — X-rays: general

1. INTRODUCTION

Anomalous X-ray pulsars are an unusual class of astrophysical objects. There are currently only five confirmed AXPs: 4U 0142+61, 1E 1048.1–5937, 1E 1841–045, RXS J170849.0–400910 (hereafter 1RXS 1708–4009), and 1E 2259.1+586. All five are located in the Galactic

[1]Department of Physics, Rutherford Physics Building, McGill University, 3600 University Street, Montreal, Quebec, H3A 2T8, Canada

[2]Department of Physics and Center for Space Research, Massachusetts Institute of Technology, Cambridge, MA 02139

[3]Alfred P. Sloan Research Fellow

plane and two (1E 2259.1+586 and 1E 1841–045) are coincident with supernova remnants. A sixth AXP candidate, AX J1845.0–0258, is also coincident with a supernova remnant (Gaensler et al. 1999).

The observational properties of AXPs (see Israel et al. 2002, for a review) are generally quite different from those of conventional accreting binary X-ray pulsars (see Bildsten et al. 1997, and references therein for a compendium of accreting X-ray pulsar properties). In particular, AXPs have spin periods in the narrow 6–12 s range, while accreting X-ray pulsars have periods that span 0.002–1400 s. AXPs have luminosities in the narrow range $10^{34} - 10^{36}$ erg s^{-1}. By comparison, typical accreting X-ray pulsars are extremely variable, with luminosities spanning a much broader range ($10^{34} - 10^{39}$ erg s^{-1}). AXP spectra are considerably softer than those of the typical accreting pulsar. Accreting pulsar spectra are generally well described as a power law with a cut-off in the 10–20 keV range. AXP spectra, by contrast, are generally characterized by a blackbody spectrum of energy $kT \simeq 0.35 - 0.6$ keV, with a hard energy excess that can be characterized by a steep power law of index -2 to -4. The timing properties of AXPs also contrast sharply with those of most accreting pulsars. All of the known AXPs, as we show in this paper, appear to be undergoing steady, prolonged spin-down, though some are more steady than others. By comparison, most accreting pulsars are spinning up (on average), or alternating between spin-up and spin-down, and have poor rotational stability.

Most importantly, the AXPs show no evidence for a binary companion. Specifically, the limits on the X-ray/optical flux ratio in AXPs rule out the presence of massive companions as in the conventional high-mass X-ray binaries (e.g. Mereghetti et al. 1992; Corbet & Mihara 1997; Israel et al. 1999a). In addition, careful pulse timing of AXPs has failed to detect any evidence for binary motion of the neutron star on time scales of a few minutes to several days (Mereghetti et al. 1998; Wilson et al. 1999). The limits imply that only extremely low-mass companions are allowed in these systems, unless we are observing all AXPs face-on, which is unlikely. Furthermore, mass-transferring low-mass companions are also unlikely because the supernova remnant associations imply youth, and because these systems rarely survive the supernova.

Currently, models for AXPs fall into two distinct categories. One class of models is that AXPs are young, isolated, ultra-magnetized neutron stars or "magnetars" (Thompson & Duncan 1996; Heyl & Hernquist 1997). If the spin-down of the pulsar is primarily due to magnetic dipole radiation, then the AXPs have enormous surface magnetic dipolar fields, in the range $B \sim 10^{14} - 10^{15}$ G. The identification with magnetars is further strongly motivated by the similarity of the AXP emission to that of the soft gamma-ray repeaters (SGRs) in quiescence. Specifically, the latter have similar pulse periods, are spinning down (Kouveliotou

et al. 1998; Kouveliotou et al. 1999), and have X-ray spectra that are comparable to, though somewhat harder than, those of the AXPs, at least when not in outburst (Mereghetti et al. 2000; Kulkarni et al. 2001). Independent evidence for the ultra-high magnetic fields exists in SGRs; for example, a $\sim 10^{15}$ G magnetic field is required to contain the radiation that is seen following major outbursts (Thompson & Duncan 1995; Thompson & Duncan 1996).

The second category of model proposed to explain AXP emission is that they are accreting from a disk of material leftover from the supernova explosion that created the neutron star (Chatterjee et al. 2000; Alpar 1999; Marsden et al. 2001). Fall-back disks around neutron stars have been proposed in other contexts (Michel 1988); here, the AXPs represent a single, short-lived phase in the evolution of a neutron star having magnetic field only slightly larger than those of radio pulsars. In this phase, the neutron star is in a propeller mode in which the inner edge of the accretion radius lies between the magnetospheric and corotation radii. This model, in its original version (Perna et al. 2000), significantly overpredicted the expected optical/IR flux from the fall-back disk (Hulleman et al. 2000a,b; Kaplan et al. 2001). A more recent version includes the effects of a thermal disk instability which may prevent the disk from expanding radially, hence allowing it to remain sufficiently dim to be consistent with the optical/IR limits (Menou et al. 2001). Nevertheless, difficulties remain with the accretion model. In particular, although the noise properties of a fall-back disk are currently unknown, the extremely steady spin down of two AXPs (Kaspi, Chakrabarty & Steinberger 1999) is at odds with that seen in most X-ray pulsars that definitely have accretion disks (but see Baykal et al. 2001). Furthermore, very noisy timing behavior seen in one AXP (1E 1048.1–5937) shows no evidence for correlated flux variations, as are expected in fall-back disk accretion models (Kaspi et al. 2001).

In this paper, we present a variety of observational results from our program of regular monitoring observations of AXPs with the *Rossi X-ray Timing Explorer*. We make use of dedicated as well as archival monitoring observations spanning several years for three AXPs. Initial results from this program were presented elsewhere (Kaspi et al. 1999, Kaspi, Lackey & Chakrabarty 2000) and focused on the timing properties of 1RXS 1708–4009 and 1E 2259.1+586. Kaspi et al. (2001) and Gotthelf et al. (2001) present results for AXPs 1E 1048.1–5937 and 1E 1841–045, respectively. In this paper, we report for the first time on 4U 0142+61, and update timing results for 1RXS 1708–4009 and 1E 2259.1+586. In addition, we use the same data sets to study pulse morphology variability and energy dependence, as well as the stability of the pulsed flux. Our goal is to clarify important observational properties of AXPs in the hope of offering new, quantitative data for use in testing AXP models.

2. OBSERVATIONS

The results presented here were obtained using the Proportional Counter Array (PCA; Jahoda et al. 1996) on board the Rossi X-ray Timing Explorer (*RXTE*). The PCA consists of an array of five collimated xenon/methane multi-anode proportional counter units operating in the 2 – 60 keV range, with a total effective area of approximately 6500 cm^2 and a field of view of $\sim 1^{\rm o}$ FWHM. Our observations consist primarily of short snapshots taken on a monthly basis (see Table 1). In addition, we used a handful of archival observations; the exposures in these observations vary from very short ($T \simeq 1$ ks) to very long ($T \simeq 20-40$ ks; see Table 1). We used the `GoodXenonwithPropane` data mode, which records photon arrival times with 1-μs resolution and bins energies into one of 256 channels. Due to the soft spectrum of these sources, we analyzed only events from the top xenon layer of each PCU. Photon arrival times at each epoch were adjusted to the solar system barycenter, and binned with 31.25-ms time resolution.

3. ANALYSIS AND RESULTS

3.1. Phase Coherent Timing

In the timing analysis, we included only those events having energies in a predetermined range so as to maximize the signal-to-noise ratio of the pulse. The energy cuts used were 2.5 – 9.0 keV for 4U 0142+61 and 1E 2259.1+586 and 2.2 – 5.5 keV for 1RXS 1708–4009. Each binned time series was epoch-folded using the best estimate frequency determined initially from either a periodogram or Fourier transform (though later folding was done using the timing ephemeris determined by maintaining phase coherence; see below). Resulting pulse profiles were cross-correlated in the Fourier domain with a high signal-to-noise template created by adding phase-aligned profiles from previous observations. The templates are shown in Figure 1 along with their respective Fourier transforms in Figure 2. The cross-correlation returns an average pulse time-of-arrival (TOA) for each observation corresponding to a fixed pulse phase. The pulse phase ϕ at any time t can be expressed as a Taylor expansion,

$$\phi(t) = \phi(t_0) + \nu_0(t-t_0) + \frac{1}{2}\dot{\nu}_0(t-t_0)^2 + \frac{1}{6}\ddot{\nu}_0(t-t_0)^3 + \cdots, \quad (1)$$

where $\nu \equiv 1/P$ is the pulse frequency, $\dot{\nu} \equiv d\nu/dt$, etc., and subscript '0' denotes a parameter evaluated at the reference epoch $t = t_0$. The TOAs were fit to the above polynomial using

the pulsar timing software package TEMPO[4]. Unambiguous pulse numbering is made possible by obtaining monitoring observations spaced so that the best-fit model parameters have a small enough uncertainty to allow prediction of the phase of the next observation to within ~ 0.2. Typically this requires two closely spaced observations (within a few of hours of each other) followed by one spaced a few days later, and regular monitoring thereafter, as long as phase coherence can be maintained.

To minimize use of telescope time while maximizing precision, our monitoring data consisted of frequent brief snapshots of each pulsar (Table 1). These snapshots suffice to measure TOAs to good precision. However, at each epoch, the period as determined by a Fourier Transform or epoch-folding has typical uncertainty of a few milliseconds. Thus, snapshots can determine spin parameters with high precision only when phase coherence can be maintained.

For 4U 0142+61, we report here for the first time a phase-coherent timing solution that indicates that this AXP has been an extremely stable rotator over 4.4 yr of *RXTE* monitoring. However, a 2-yr gap in the data precludes unambiguous absolute pulse numbering; we find two equally viable phase-connections that differ by one pulse. Unambiguous phase count can be maintained in 1.3 and 1.4-yr segments at the beginning and end of the 4.4-yr span, respectively. Phase residuals after subtraction of spin-down models that include ν and $\dot{\nu}$ only in the first and second segments have RMS of 2.7% and 1% of the pulse period, respectively, and are featureless. The best-fit model parameters for each segment, as well as the two indistinguishable models for the entire 4.4-yr span, are given in Table 2. Timing residuals for solution "A" (see Table 2) are shown in Figure 3; those for solution "B" are qualitatively similar.

It is interesting to compare our results with frequency measurements made for this pulsar with various X-ray telescopes over the past ∼20 yr. Figure 4 shows these data (taken from Israel et al. 1999b) along with our *RXTE* ephemeris. The top panel shows ν versus time; the thick solid line is our phase-connected ephemeris (the distinction between A and B is not visible on this plot) over the 4.4-yr span *RXTE* has monitored it, while the thin line is the extrapolation of our ephemeris backward. The uncertainties are smaller than the thickness of the lines. The bottom panel shows the same data but with the linear and offset trend removed. All but one data point (taken with EXOSAT) agree with the back-extrapolation. That one point suggests that the pulsar may exhibit deviations from a simple spin-down law; these could be due to random noise processes or glitches. Further observations can test this.

For 1RXS 1708–4009, phase coherent timing has been accomplished in the 1.4 yr since

[4]http://pulsar.princeton.edu/tempo

the glitch reported by Kaspi et al. (2000). In these data, we find a significant positive $\ddot{\nu}$ (see Table 3). This indicates a decay of the negative $\dot{\nu}$, expected for long-term glitch recovery, as seen in glitching radio pulsars (e.g. Shemar & Lyne 1996). Phase residuals after subtraction of the best fit model are shown in Figure 5. We note that the value for $\dot{\nu}$ reported in Table 2 is different by 3.8σ from that reported by Kaspi et al. (2000). This is likely due to the unmodeled influence of $\ddot{\nu}$ in the earlier, shorter data set.

The rotational stability of 1E 2259.1+586, first reported by Kaspi et al. (1999), has now persisted over 4.5 yr, although the inclusion of $\ddot{\nu}$ has been necessary. Phase residuals after subtraction of a simple model that includes only ν, $\dot{\nu}$ and $\ddot{\nu}$ have RMS under 1% of the pulse period (see Table 3, Fig. 5). We note the presence of very low-level systematic trends in the most recent data; their origin is unknown.

3.2. Pulse Morphology Changes

To search for pulse profile changes, the profiles were first phase aligned using the templates and the same cross-correlation procedure used for timing. Each data profile (D) was fit to the template (T) by adjusting two parameters, $\mathcal{F}$ and $\mathcal{DC}$, to minimize a χ^2 statistic, where

$$\chi^2_\nu = \frac{1}{N_\phi - 4} \sum_{i=1}^{N_\phi} \frac{(D_i - (\mathcal{F} \cdot T_i - \mathcal{DC}))^2}{\sigma^2_{D_i} + \mathcal{F}^2 \cdot \sigma^2_{T_i}}. \quad (2)$$

Here N_ϕ is the number phase bins, and σ_D and σ_T are the errors associated with D and T, respectively. The resulting data profile was subtracted from the template to yield "profile residuals" for each observation.

To search for pulse profile variations, using the optimal $\mathcal{F}$ and $\mathcal{DC}$, we calculated the probability of each χ^2_ν statistic given their expected distribution and the number of degrees of freedom ($\nu = N_\phi - 4$). The procedure was repeated for each pulsar with $N_\phi = 8, 16, 32$ in order to have sensitivity to a variety of types of pulse profile changes. We have not detected any large pulse profile variations. This justifies our other analysis procedures which assume a fixed profile. However, in a handful of observations, we have found evidence for low-level pulse profile changes, at the $\sim 3\sigma$ level for all three sources. These are intriguing; however at this level, they require confirmation using longer monitoring observations.

It is difficult to set quantitative upper limits on the amplitude of pulse profile changes to which we were sensitive, as these depend on the shape of the change, and vary depending

on the length of the observation. Typically, RMS profile residuals are ∼20% of the pulse peak, although this varied from 4–40%.

Iwasawa et al. (1992) reported a significant change in the pulse morphology of 1E 2259.1+586 in 1.2–14 keV *GINGA* observations obtained in 1990, such that the leading pulse had amplitude roughly half that of the trailing pulse (compare with Fig. 1C). If correct, this has important implications for the magnetar model, which only predicts such pulse morphology changes in the event of a restructuring of the magnetic field, as might occur following a major SGR-like outburst. Although it is difficult to quantify upper limits on the amplitude of pulse profile changes generally, we have done Monte Carlo simulations to see whether we were sensitive to the same change observed by Iwasawa et al. (1992). In particular, using the original 1990 *GINGA* pulse profile (kindly supplied to us by B. Paul and F. Nagase) with random Poisson-deviated noise added, we repeated our pulse change morphology analysis as described above. Our simulations show that we would have detected the change with high (>99%) confidence in 25% of our observations (those with integration times $\gtrsim$10 ks), and with moderate (>90%) confidence in 45% of our observations (those with integration times of $\gtrsim$7 ks; see Table 1).

3.3. Pulse Profile Energy Dependence

AXP spectra are generally best fit by a two-component model consisting of a photo-electrically absorbed blackbody with a hard power-law tail (Israel et al. 1999b). Whether these two components are physically distinct is an open question . To investigate this, we compared the pulse profile morphology in two energy bands, 2–4 keV and 6–8 keV. These were chosen because the 2–4 keV band has a significant blackbody component ($\sim 40\% - 60\%$ of total flux, depending on source and model) and the 6–8 keV band is greatly dominated by the power-law component ($\gtrsim$ 95% of total flux). (see Özel et al. 2001)

Figure 7 display the average pulse profiles of 4U 0142+61, 1RXS 1708–4009 and 1E 2259.1+586 in the energy bands 2–4 keV and 6–8 keV. Note that the scaling in these plots was chosen to minimize the χ^2 of the difference between the soft and hard profiles. Thus the only information that these plots convey is the relative amplitudes of the features of the profile. The minimization of the χ^2 statistic (Eq. 2) between profiles in the two energy bands was done in the same manner as for the pulse morphology changes (see §3.2).

Another way of characterizing the pulse morphology as function of energy is to consider the pulse profile harmonic content in different energy bands. Figure 8 displays the power of the $n^{\rm th}$ harmonic (A_n) in units of total power in the remaining harmonics (A_{total} =

$A_1 + A_2 + \cdots + A_{\frac{N_\phi}{2}}$, where N_ϕ is the number of phase bins), versus harmonic number n, for each source.

From Figure 7 and 8 it is clear that all three of the AXP pulse profiles vary significantly as a function of energy, but to different degrees.

3.4. Pulsed Flux Time series

Given the large field-of-view of the PCA, the low count rates for the sources relative to the background, and the fact that, for example, 1E 2259.1+586 is in a supernova remnant, total flux measurements are difficult with our *RXTE* data. Instead, we have determined the pulsed component of the flux, by using the off-pulse emission as a background estimator.

Data from each observing epoch were folded at the expected pulse period as was done for the timing analysis. However, for the flux analysis, 16 phase bins were used across the pulse. For each phase bin, we maintained a spectral resolution of 128 bins over the PCA range. Given the broad morphologies of the average pulse profile, only one phase bin could be used as a background estimator. The pulse profiles were then phase aligned, so that the same off-pulse bin was used for background in every case. The remaining phase bins were summed, and their spectral bins regrouped using the `FTOOL grppha`, such that no bin had fewer than 20 counts after background subtraction. Energies below 2 keV and above 10 keV were ignored, leaving 17–21 spectral channels for fitting, depending on the data set. The regrouped, phase-summed data sets, along with the background measurement, were used as input to the X-ray spectral fitting software package `XSPEC`[5]. Not all PCUs were on during our observations, but this was taken into account when producing response matrices. Response matrices were created using the `FTOOL`s `xtefilt` and `pcarsp`. Because of the limited spectral resolution, fitting a two-component model was not practical, so we used a simple photoelectrically absorbed power-law, at first holding only N_H fixed (see Table 4). For all sources we found that the photon index Γ was constant within the uncertainties; we therefore held it fixed at its mean value. To extract a pulsed flux at each observing epoch we refitted each spectrum by varying only the normalization. Uncertainties were measured using the `XSPEC` command `steppar`. Our flux time series for 4U 0142+61, 1RXS 1708–4009 and 1E 2259.1+586 are displayed in Figures 9, 10 and 11 respectively. We do not find evidence for any large variability in the pulsed flux. Although the measured χ^2_ν statistics for 1E 2259.1+586 and 1RXS 1708–4009 are significantly larger than unity, given that the error

[5]http://xspec.gsfc.nasa.gov

bars are statistical only, we cannot rule out unmodeled systematic errors. A long-term flux monitoring campaign with an imaging telescope is obviously desirable.

4. Discussion

4.1. Timing

With our report of successful phase-coherent timing for 4U 0142+61, the detailed long-term timing properties of all known AXPs are becoming clear. As a population, they are generally spinning down steadily and with impressive stability. Indeed, for 1E 2259.1+586, the stability is comparable to that of many radio pulsars: the Δ_8 statistic (defined as the phase deviation due to $\ddot{\nu}$ after 10^8 s; see Arzoumanian et al. 1994) is 0.43, consistent with what would be expected for a radio pulsar having a comparable spin-down rate, -0.78, given the large scatter in the radio pulsar values. For 4U 0142+61, fitting for $\ddot{\nu}$ in either of the two best solutions yields $|\ddot{\nu}| = (5 \pm 1) \times 10^{-24}$ s^{-3}, implying $\Delta_8 = 0.89$, slightly larger than that expected for a radio pulsar with the same spin-down rate, -0.42, though still comparable given the scatter. For 1RXS 1708–4009, Δ_8 is significantly higher than would be predicted (2 versus 0.2), however this is consistent with glitch recovery.

The stability of 1E 2259.1+586 is particularly surprising given past reported large deviations from simple spin-down (e.g. Baykal & Swank 1996). This is in contrast to 1E 1048.1–5937 which also showed apparent deviations from simple spin-down (see, e.g. Oosterbroek et al. 1998; Paul et al. 2000) but which we have verified in *RXTE* monitoring (Kaspi et al. 2001). As argued by Baykal et al. (2000), it may be a coincidence that 1E 2259.1+586 has shown great rotational stability during our observations only (but see also § 4.4).

The current stability of 1E 2259.1+586 allows for a test of the Melatos (1999) model of radiative precession. In that model, given well-defined but uncertain assumptions about the geometry and location of the magnetic field, a highly magnetized neutron star could deviate from sphericity and exhibit significant precession with period of a few years. This was suggested as an explanation for timing anomalies seen for 1E 2259.1+586 and 1E 1048.1–5937. The current data for 1E 2259.1+586 rule out, with 99% confidence, an amplitude for precession 0.013 times that used by Melatos (1999) to explain the timing anomalies. Radiative precession was also ruled out by *RXTE* monitoring for 1E 1048.1–5937 (Kaspi et al. 2001). Frequent large glitches in both these sources, as were suggested by Heyl & Hernquist (1999), also have not been confirmed. Also, neither 4U 0142+61 and 1E 1841–045 (Gotthelf et al. 2001) show any evidence for either radiative precession or frequent large glitches.

Overall, however, a striking property of the timing of the AXPs as a whole, apart from the stability, is the diversity of behavior. 1E 2259.1+586 and 4U 0142+61 have shown great stability; 1E 1841–045 shows stability but with considerably more red noise (Gotthelf et al. 2001); 1RXS 1708–4009 has exhibited a glitch with recovery similar to what is observed for radio pulsars; and 1E 1048.1–5937 is less stable than even some known accretors (Kaspi et al. 2001).

Interestingly, there is a correlation between timing stability and $\dot{\nu}$ in our data. The sources with by far the smallest $\dot{\nu}$'s, 1E 2259.1+586 and 4U 0142+61, are the most stable (at least during our observations), while that with the largest, 1E 1048.1–5937, is the least so. The SGRs, being even less stable (Woods et al. 2000; Woods et al. 2001), have even larger $\dot{\nu}$'s, in agreement with this trend. 1E 1841–045 and 1RXS 1708–4009 have timing stabilities and $\dot{\nu}$ intermediate between the extremes. One therefore might expect 1E 1841–045 to exhibit a glitch in the near future. If correct, the trend suggests a continuum of timing properties between the AXP and SGR populations, lending additional support to the connection between them. Furthermore, it has long been recognized that radio pulsar timing stability is also correlated with spin-down rate (e.g. Cordes & Helfand 1980; Arzoumanian et al. 1994). This suggests, in addition, a connection between all three populations, and a continuum of timing behavior that depends on stellar magnetic field. If correct, this provides strong support for the magnetar model.

Marsden & White (2001) noted a correlation between spin-down rate and spectral properties in AXPs. An additional correlation with timing stability could strengthen the argument that the spin properties, emission mechanisms, and internal structure and dynamics are all related in these objects.

4.2. Pulse Morphology

The presence of substantial harmonic content in AXP pulse profiles (see Fig. 8) is at odds with models in which the X-ray emission is thermal from the surface of a hot neutron star having conventional magnetic field. As shown by Dedeo et al. (2001), the expected range of ratios of second to first Fourier amplitudes, A_2/A_1, can be predicted for a neutron star emitting thermal X-rays, as a function of total pulse fraction, for different radially peaked beaming functions, surface hot-spot geometries, and neutron star compactnesses. Low harmonic content is expected primarily because of gravitational light bending, unless there is significant beaming. Given the pulsed fraction of 1E 2259.1+586 (Özel et al. 2001, and references therein), Dedeo et al. (2001) show that the ratio of $A_2/A_1 \leq 1$ for all possible geometries and compactnesses, while Figure 8C shows $A_2/A_1 = 3.97 \pm 0.01$ in the soft 2–

4 keV band. The presence of a significant third harmonic in 1RXS 1708–4009 (Fig. 8B) and even a significant sixth harmonic in 1E 2259.1+586 (Fig. 8C) is similarly problematic. On the other hand, Özel (2001) suggests that, in the magnetar model, when properly accounting for the propagation of X-rays through the neutron star atmosphere, the pulse morphology can be surprisingly non-sinusoidal. In particular, in $10^{14} - 10^{15}$ G magnetic fields, the emission from a surface patch can be highly and non-radially beamed. Furthermore, if the surface distribution itself is non-isotropic, AXP profiles may be reproduceable. Indeed, Özel, Psaltis & Kaspi (2001) show that AXP pulsed fractions and luminosities can only be reproduced, assuming thermal emission from the surface of a magnetar propagating through a hydrogen atmosphere, with a single hot spot. In addition, Thompson, Lyutikov & Kulkarni (2001) argue that AXP pulse profiles can be accounted for even if the surface emission were isotropic, because of resonant scattering off charged particles in the magnetosphere, which has anisotropic optical depth. A detailed comparison of model predictions with observed AXP pulse profiles may prove interesting.

4.3. Pulse Morphology Energy Dependence

The energy dependence of the pulse profiles of AXPs can in principle be a strong constraint on the emission model. We have studied this by comparing the morphologies of pulse profiles in two energy bands. The AXPs display a variety of behaviors in this regard. For example, while 1E 1048.1–5937 and 1E 1841–045 show essentially no change in pulse morphology with energy (Kaspi et al. 2001; Gotthelf et al. 2001), 1RXS 1708–4009 shows tremendous variation (Fig. 7B). In no case (except possibly 1RXS 1708–4009) are the profiles in the two energy bands very different, problematic for interpreting AXP two-component spectra as being a result of two independent emission mechanisms (e.g. Perna et al. 2001). Figure 7A shows a possible energy-dependent phase lag, in which the low energy pulse lags the high energy pulse, however, this is not observed in any other AXP.

There is a possible rough trend in which sources with the least harmonic content (1E 1048.1–5937, 1E 1841–045) show the least energy dependence. However the lack of strong pulse morphology evolution with energy in 1E 2259.1+586 compared with 1RXS 1708–4009 does not obviously support this. Another possibly interesting trend is that for the sources in which the ratio of the Fourier amplitudes of the second and first harmonics is large (1E 2259.1+586, 4U 0142+61), the ratio is largest at low energies. This manifests itself in the profile plots as the ratio of peak heights being closer to unity in the hard band than in the soft, which is true of 1RXS 1708–4009 as well.

Whether and how these observations can constrain models remains to be seen. Özel

(2001) shows that, when photon propagation through a magnetar atmosphere is properly modeled, the angular dependence of the emission has two components: a narrow pencil beam at small angles with respect to the surface normal, and a broad fan beam at large angles. She shows that the importance and opening angle of the pencil beam increases with increasing photon energy. This may be able explain the observed change in the relative peak amplitudes as a function of photon energy, especially in 1RXS 1708–4009, if part of the pulse is from a fan beam and part from a pencil beam. However detailed pulse profile modeling is required.

4.4. Pulsed Flux Time Series

The pulsed fluxes of all known AXPs are roughly constant, with RMS fluctuations of at most ∼20–30% of the mean (1σ) (see Table 4, Kaspi et al. 2001, Gotthelf et al. 2001). Past studies of the flux stability of two AXPs, 1E 2259.1+586 and 1E 1048.1–5937, have suggested that their phase-averaged fluxes are highly variable, with fluctuations possibly as large as a factor of ten (Baykal & Swank 1996; Oosterbroek et al. 1998). Large flux variations, particularly on time scales under a year and in the absence of torque variations, are unexpected in the magnetar model. This is because in this model, X-rays come from the hot surface where the heat is maintained by the decay of the interior magnetic field. As the thermal conduction time from core to surface is roughly a year (Van Riper et al. 1991), flux variations on shorter time scales are hard to explain in the absence of burst activity as is seen in the SGRs (e.g. Woods et al. 2001).

With the caveat that we measure pulsed flux while other studies measured total flux, it is surprising that we find such flux stability in our observations given past claims. Baykal et al. (2000) argued that the flux stability of 1E 2259.1+586 is a result of its currently being in a quiescent accreting state that is also characterized by timing stability (see also § 4.1). Though we cannot rule this out, we point out that (i) the same coincidence would have to be true of 1E 1048.1–5937 for flux stability, (ii) the pulsed fluxes of 4U 0142+61, 1RXS 1708–4009 and 1E 1841–045 are also stable, and (iii) the pulsed flux of 1E 1048.1–5937 is stable even though it shows unstable timing behavior, which argues that the flux stability is independent of spin-down behavior. We note that our flux measurements, in contrast to past studies, have been made using a single instrument, single bandpass, and analysis method, which eliminates the difficulty in comparing measurements made with different instruments, different spectral ranges, and different analysis methods.

Vasisht et al. (2000) have suggested that the variable X-ray pulsar AX J1845.0–0258 which is at the center of the supernova remnant G29.6+0.1 may also be an AXP. This source has shown variations in its X-ray luminosity by a factor of ∼10 between observations taken

6 yr apart. Given that the pulsed fluxes of all known AXPs are stable, the interpretation of AX J1845.0–0258 as a *bona fide* AXP is therefore questionable.

5. Conclusions

We have presented a variety of observational results for three anomalous X-ray pulsars, 4U 0142+61, 1RXS 1708–4009 and 1E 2259.1+586, obtained using regular monitoring observations and archival observations from the PCA aboard *RXTE*. Our results, combined with those for 1E 1048.1–5937 and 1E 1841–045 (Kaspi et al. 2001; Gotthelf et al. 2001), provide significantly improved descriptions of AXP X-ray properties that can be used to test models for the nature of these sources.

Specifically, with our successful phase-coherent timing of 4U 0142+61, the detailed timing properties of all known AXPs are now established and can be compared. We find a wide variety of timing behaviors, ranging from high stability (in 1E 2259.1+586 and 4U 0142+61), to instabilities so severe that phase-coherent timing is not possible (in 1E 1048.1–5937). We note that timing stability appears correlated with decreasing $\dot{\nu}$. If this trend is real, it suggests a continuum of timing properties between the AXP and SGR populations, lending additional support to the connection between them. We note that a correlation between timing instability and spin-down rate has long been recognized among radio pulsars (e.g. Cordes & Helfand 1980; Arzoumanian et al. 1994), suggesting a connection between all three populations.

We have also used the *RXTE* data to investigate a variety of other AXP properties. Motivated by a report of a significant change in pulse morphology in 1E 2259.1+586 in 1990 (Iwasawa et al. 1992), we searched for changes in the pulse morphology at each epoch for all targets. We find no significant pulse morphology variations. Typically, we rule out variations in features having amplitude $\gtrsim$20% of the peak amplitude at the 1σ level, although the limit depends on source and integration time.

We have presented high signal-to-noise average pulse profiles for each AXP, and considered them as a function of energy. We show that, as in the timing properties, there is a variety of different behaviors for the energy dependence. Possible trends include a greater energy dependence for pulses profiles having greater harmonic content, and, for the latter sources, relative peak amplitudes tending closer to unity as photon energy increases. Detailed modeling of AXP pulse profiles, in addition to their pulsed fractions and luminosities (Özel et al. 2001) can test models in which the emission is from the surface of a cooling magnetar (Özel 2001; Ho & Lai 2001; Zane et al. 2001).

Finally, we use the monitoring and archival data to obtain pulsed flux time series for each source. We have found no large changes in pulsed flux for any source, and have set 1σ upper limits on variations $\sim$20–30% (depending on the source). This is surprising given previous reports of large (factor of 5–10) total flux variations in 1E 2259.1+586 and 1E 1048.1–5937 (Baykal & Swank 1996; Oosterbroek et al. 1998). Assuming a constant pulsed fraction, this suggests that more than one of the AXPs happen to be much more quiescent during the *RXTE* monitoring than in the past.

We are grateful to D. Chakrabarty, M. Lyutikov, M. Muno, F. Özel, D. Psaltis, M.S.E. Roberts and C. Thompson for useful discussions. We also thank B. Paul and F. Nagase for assistance in obtaining the *Ginga* data. This work was supported in part by a NASA LTSA grant (NAG5-8063) and an NSERC Research Grant (RGPIN228738-00) to VMK, with additional support from a NASA ADP grant (NAG 5-9164). This research has made use of data obtained through the High Energy Astrophysics Science Archive Research Center Online Service, provided by the NASA/Goddard Space Flight Center.

REFERENCES

Alpar, M. A. 1999, http://xxx.lanl.gov/abs/astro-ph/9912228

Arzoumanian, Z., Nice, D. J., Taylor, J. H., & Thorsett, S. E. 1994, ApJ, 422, 671

Baykal, A., Inam, C., Alpar, M. A., in't Zand, J., & Strohmayer, T. 2001, MNRAS, submitted

Baykal, A., Strohmayer, T., Swank, J., Alpar, A., & Stark, M. J. 2000, MNRAS, 319, 205

Baykal, A. & Swank, J. 1996, ApJ, 460, 470

Bildsten, L., Chakrabarty, D., Chiu, J., Finger, M. H., Koh, D. T., Nelson, R. W., Prince, T. A., Rubin, B. C., Scott, D. M., Stollberg, M., Vaughan, B. A., Wilson, C. A., & Wilson, R. B. 1997, ApJS, 113, 367

Brandt, N. & Podsiadlowski, P. 1995, MNRAS, 274, 461

Chatterjee, P., Hernquist, L., & Narayan, R. 2000, ApJ, 534, 373

Corbet, R. H. D. & Mihara, T. 1997, ApJ, 475, L127

Cordes, J. M. & Helfand, D. J. 1980, ApJ, 239, 640

Dedeo, S., Psaltis, D., & Narayan, R. 2001, ApJ, 559, 346

Fahlman, G. G. & Gregory, P. C. 1981, Nature, 293, 202

Gaensler, B. M., Gotthelf, E. V., & Vasisht, G. 1999, ApJ, 526, L37

Gotthelf, E. V., Gavriil, F., Kaspi, V. M., Vasisht, G., & Chakrabarty, D. 2001, ApJ, in press

Heyl, J. S. & Hernquist, L. 1997, ApJ, 489, L67

Heyl, J. S. & Hernquist, L. 1999, MNRAS, 304, L37

Ho, W. C. G. & Lai, D. 2001, MNRAS, submitted

Hulleman, F., van Kerkwijk, M., Verbunt, F. W. M., & Kulkarni, S. R. 2000a, A&A, 358, 605

Hulleman, F., van Kerkwijk, M. H., & Kulkarni, S. R. 2000b, Nature, 408, 689

Israel, G., Mereghetti, S., & Stella, L. 2002 (Memorie della Societa' Astronomica Italiana), in press

Israel, G. L., Covino, S., Stella, L., Campana, S., Haberl, F., & Mereghetti, S. 1999a, ApJ, 518, L107

Israel, G. L., Oosterbroek, T., Angelini, L., Campana, S., Mereghetti, S., Parmar, A. N., Segreto, A., Stella, L., Van Paradijs, J., & White, N. E. 1999b, A&A, 346, 929

Iwasawa, K., Koyama, K., & Halpern, J. P. 1992, PASJ, 44, 9

Jahoda, K., Swank, J. H., Giles, A. B., Stark, M. J., Strohmayer, T., Zhang, W., & Morgan, E. H. 1996, Proc. SPIE, 2808, 59

Kaplan, D. L., Kulkarni, S. R., van Kerkwijk, M. H., Rothschild, R. E., Lingenfelter, R. L., Marsden, D., Danner, R., & Murakami, T. 2001, ApJ, 556, 399

Kaspi, V. M., Chakrabarty, D., & Steinberger, J. 1999, ApJ, 525, L33

Kaspi, V. M., Gavriil, F. P., Chakrabarty, D., Lackey, J. R., & Muno, M. P. 2001, ApJ, in press

Kaspi, V. M., Lackey, J. R., & Chakrabarty, D. 2000, ApJ, 537, L31

Kouveliotou, C., Dieters, S., Strohmayer, T., van Paradijs, J., Fishman, G. J., Meegan, C. A., Hurley, K., Kommers, J., Smith, I., Frail, D., & Murakami, T. 1998, Nature, 393, 235

Kouveliotou, C., Strohmayer, T., Hurley, K., Van Paradijs, J., Finger, M. H., Dieters, S., Woods, P., Thompson, C., & Duncan, R. C. 1999, ApJ, 510, L115

Kulkarni, S. R., Kaplan, D. L., Marshall, H. L., Frail, D. A., Murakami, T., & Yonetoku, D. 2001, Nature, submitted

Marsden, D., Lingenfelter, R. E., Rothschild, R. E., & Higdon, J. C. 2001, ApJ, 550, 397

Marsden, D. & White, N. E. 2001, ApJ, 551, L155

Melatos, A. 1999, ApJ, 519, L77

Menou, K., Perna, R., & Hernquist, L. 2001, ApJ, 559, 1032

Mereghetti, S., Caraveo, P., & Bignami, G. F. 1992, A&A, 263, 172

Mereghetti, S., Cremonesi, D., Feroci, M., & Tavani, M. 2000, A&A, 361, 240

Mereghetti, S., Israel, G. L., & Stella, L. 1998, MNRAS, 296, 689

Mereghetti, S. & Stella, L. 1995, ApJ, 442, L17

Michel, F. C. 1988, Nature, 333, 644+

Oosterbroek, T., Parmar, A. N., Mereghetti, S., & Israel, G. L. 1998, A&A, 334, 925

Özel, F. 2001, ApJ, submitted (astro-ph/0106071)

Özel, F., Psaltis, D., & Kaspi, V. M. 2001, ApJ, in press (astro-ph/0105372)

Paul, B., Kawasaki, M., Dotani, T., & Nagase, F. 2000, ApJ, 537, 319

Perna, R., Hernquist, L., & Narayan, R. 2000, ApJ, 541, 344

Perna, R., Heyl, J., Hernquist, L., Juett, A., & Chakrabarty, D. 2001, ApJ, 557, 18

Shemar, S. L. & Lyne, A. G. 1996, MNRAS, 282, 677

Sugizaki, M., Nagase, F., Torii, K. I., Kinugasa, K., Asanuma, T., Matsuzaki, K., Koyama, K., & Yamauchi, S. 1997, PASJ, 49, L25

Thompson, C. & Duncan, R. C. 1995, MNRAS, 275, 255

Thompson, C. & Duncan, R. C. 1996, ApJ, 473, 322

Thompson, C., Lyutikov, M., & Kulkarni, S. R. 2001, ApJ, submitted (astro-ph/0110677)

Van Riper, K. A., Epstein, R. I., & Miller, G. S. 1991, ApJ, 381, L17

Vasisht, G., Gotthelf, E., Torii, K., & Gaensler, B. M. 2000, ApJ, 542, L49

Wilson, C. A., Dieters, S., Finger, M. H., Scott, D. M., & van Paradijs, J. 1999, ApJ, 513, 464

Woods, P. M., Kouveliotou, C., Finger, M. H., Gögüs, E., Scott, D. M., Dieters, S., Thompson, C., Duncan, R. C., Hurley, K., Strohmayer, T., Swank, J., & Murakami, T. 2000, ApJ, 535, L55

Woods, P. M., Kouveliotou, C., van Paradijs, J., Finger, M. H., Thompson, C., Duncan, R. C., Hurley, K., Strohmayer, T., Swank, J., & Murakami, T. 2001, ApJ, 552, 748

Zane, S., Turolla, R., Stella, L., & Treves, A. 2001, ApJ, 560, 384

Table 1. Summary of *RXTE* Observations

Observing Period	Nominal Exposure (ksec)	Nominal Separation (weeks)	Number of Obs.	Total Exposure (ksec)
		4U 0142+61		
Mar 1996	···	···	1	7.0
Mar 1996	···	···	1	43.5
Mar 1998	···	···	1	20.3
Nov 1996 – Dec 1997	1.1	4–5	14	14.9
Mar 2000 – Feb 2001	3.3	4–5	14	46.0
Mar 2001 – Jun 2001	6.6	4–5	3	19.9
		1RXS 1708–4009		
Jan 1998 – Jan 1999	6.2	4–5	12	74.0
Feb 1999 – Jun 2001	3.1	4–5	33	103.6
May 2001	2.0	1/7	5	10.1
		1E 2259.1+586		
Sep 1996	···	···	1	86.9
Nov 1996 – Dec 1997	1.0	4–5	14	14.0
Feb 1997 – Mar 1997	24.8	1	5	124.1
Aug 1998 – Sep 1998	14.0	1	8	111.7
Jan 1999 – Mar 2001	3.2	4–5	19	61.3
Mar 2000 – May 2001	7.0	4–5	11	77.3

Table 2. Spin Parameters for 4U 0142+61.[a]

	First Span	Second Span	A	B
MJD Range	50411–50893	51610–52028	50411–52028	50411–52028
No. TOA	15	17	32	32
ν (Hz)	0.115096877(10)	0.1150969336(5)	0.1150969299(10)	0.1150969209(11)
$\dot{\nu}$ (10^{-14} Hz/s)	−2.687(5)	−2.649(11)	−2.5980(23)	−2.5969(24)
Epoch (MJD)	51704.000	51704.000	51704.000	51704.000
RMS residual	0.027	0.011	0.074	0.077

[a]Ephemerides A and B are both viable given the data set, which includes a 2-yr gap at the center of the 4.4-yr span. Ephemeris B has one additional pulse in the gap relative to Ephemeris A. See § 3.1.

Table 3. Spin Parameters for 1RXS 1708–4009 and 1E 2259.1+586.

	1RXS 1708–4009	1E 2259.1+586
MJD Range	51472–51995	50356–52016
No. TOA	19	67
ν (Hz)	0.090917063(5)	0.14328806234(8)
$\dot{\nu}$ (10^{-14} Hz/s)	−16.07(2)	−0.99434(16)
$\ddot{\nu}$ (10^{-23} Hz/s^2)	5.2(6)	0.228(14)
Epoch (MJD)	51215.9308	51995.5827
RMS residual (periods)	0.0075	0.0099

Table 4. AXP Spectral Parameters and 2-10 keV Pulsed Flux Variability Upper Limits

	Spectral Parameters			Flux Time Series Parameters		
Source	$\log N_H$ [a] (cm^{-2})	Refs. [b]	Γ [c]	χ^2_ν [d]	Degrees of Freedom	$\frac{\text{RMS flux}}{\text{mean flux}}$ [e]
4U 0142+61	22.18	1	3.50	0.63	36	0.26
1RXS 1708–4009	22.25	2	2.63	1.45	52	0.17
1E 2259.1+586	22.08	3	4.02	1.38	59	0.28

[a]For each AXP, N_H was held fixed at these values.

[b](1) Mereghetti & Stella (1995); (2) Sugizaki et al. (1997); (3) Baykal & Swank (1996).

[c]Mean power-law index as measured for the pulsed portion of the spectrum.

[d]χ^2_ν statistic of the pulsed flux time series displayed in Figures 9, 10 and 11.

[e]RMS of the pulsed flux time series displayed in Figures 9, 10 and 11 in units of the mean pulsed flux.

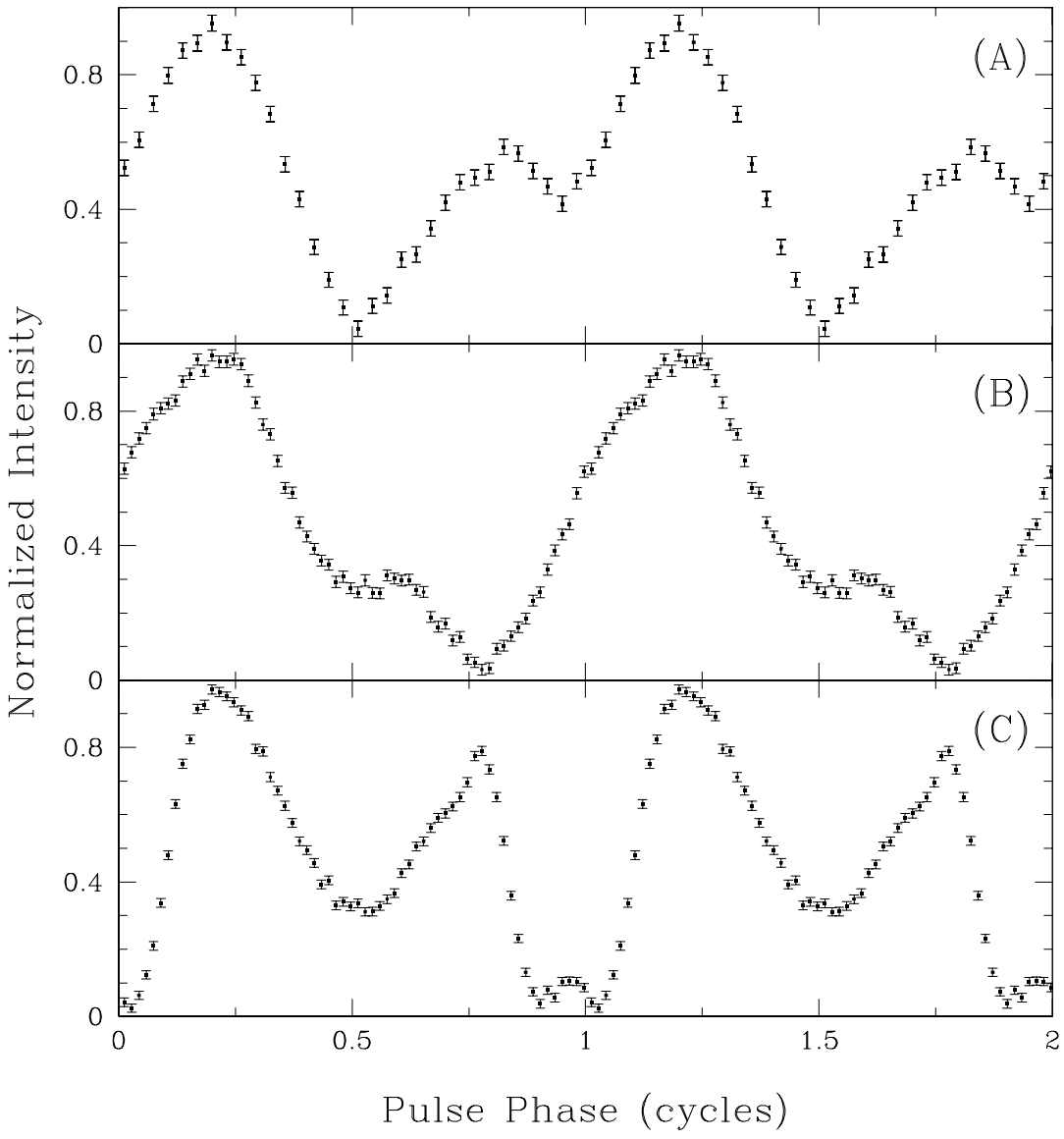

Fig. 1.— Average pulse profiles of the AXPs. Two cyles are plotted for clarity. (A) 4U 0142+61 (Total exposure time: 149 ks, energy range: 2.5 – 9.0 keV); (B) 1RXS 1708–4009 (185 ks, 2.5 – 9.0 keV); (C) 1E 2259.1+586 (469 ks, 2.2 – 5.5 keV).

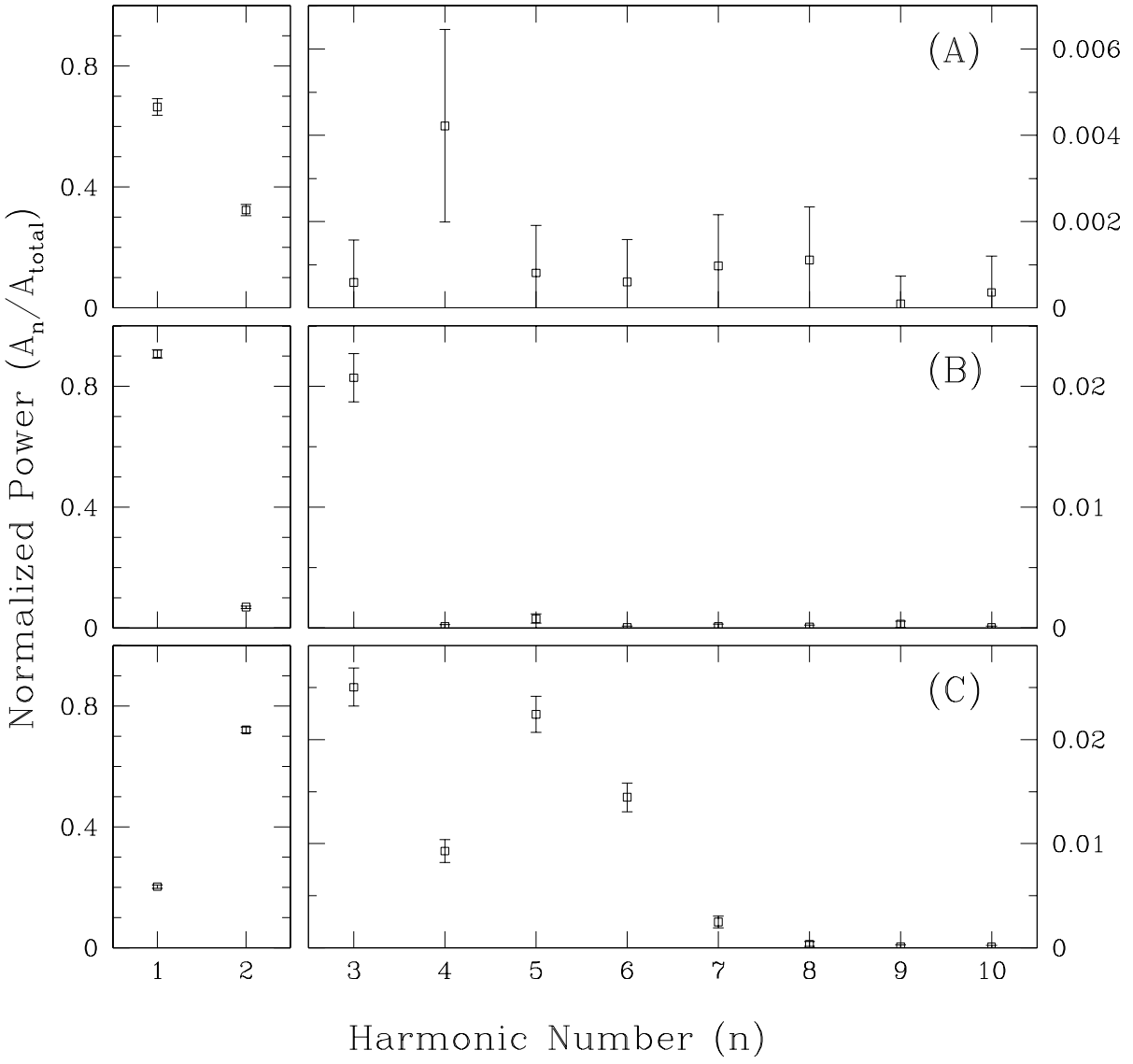

Fig. 2.— Harmonic content of the average pulse profiles in Figure 1. (A) 4U 0142+61 (Energy range: 2.5 – 9.0 keV) ; (B) 1RXS 1708–4009 (2.5 – 9.0 keV); (C) 1E 2259.1+586 (2.2 – 5.5 keV). The ratio of the power in the $n^{\rm th}$ harmonic to the total power in all harmonics is plotted versus n.

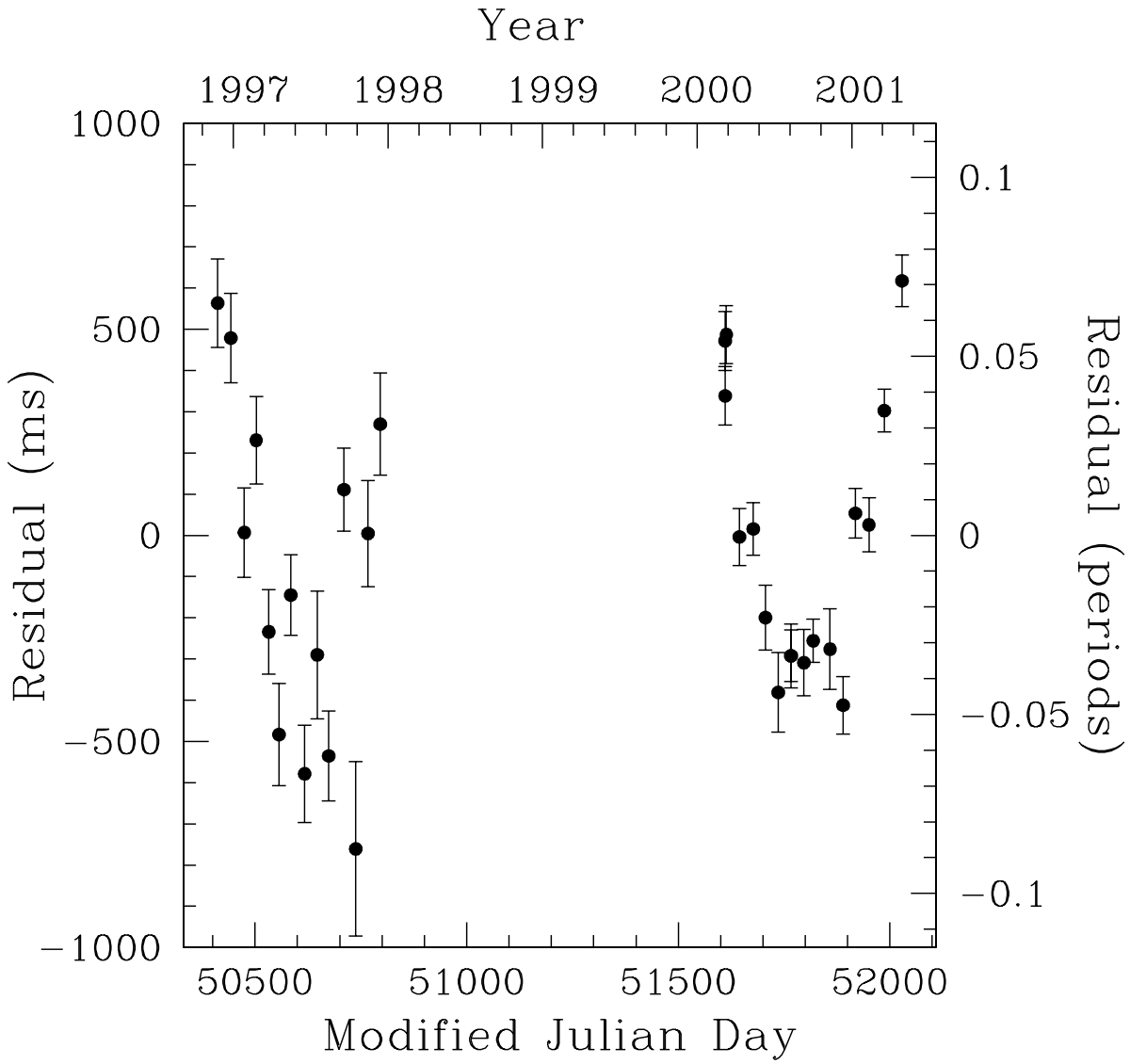

Fig. 3.— Arrival time residuals for 4U 0142+61 with Ephemeris A (Table 2), that includes ν and $\dot{\nu}$, subtracted. Residuals relative to Ephemeris B are qualitatively similar.

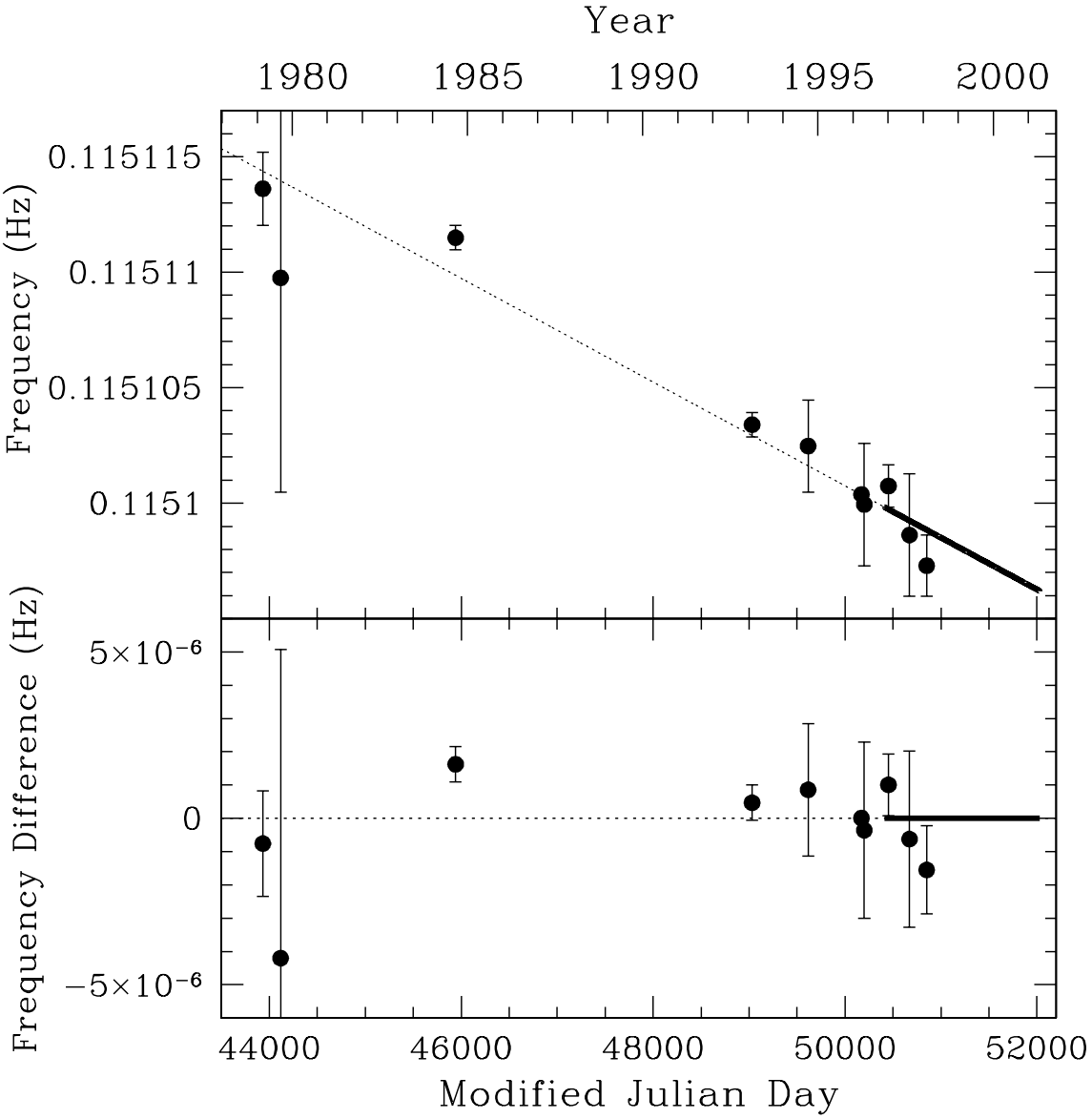

Fig. 4.— Pulse frequency history for 4U 0142+61. Top panel: the solid, thick line is the ephemeris detemined from our phase-coherent timing with *RXTE*. Individual data points are from a variety of X-ray missions (see Israel et al. 1999b for references) and are shown with 90% confidence level error bars. Note that on this scale, Ephemeris A and B (see § 3.1, Table 2) are indistinguishable. The dotted line is the extrapolation of our fit backward. Bottom panel: the same data but with the linear trend and offset removed. In both plots, the uncertainties (including that due to the ambiguity between A and B) are smaller than the width of the lines.

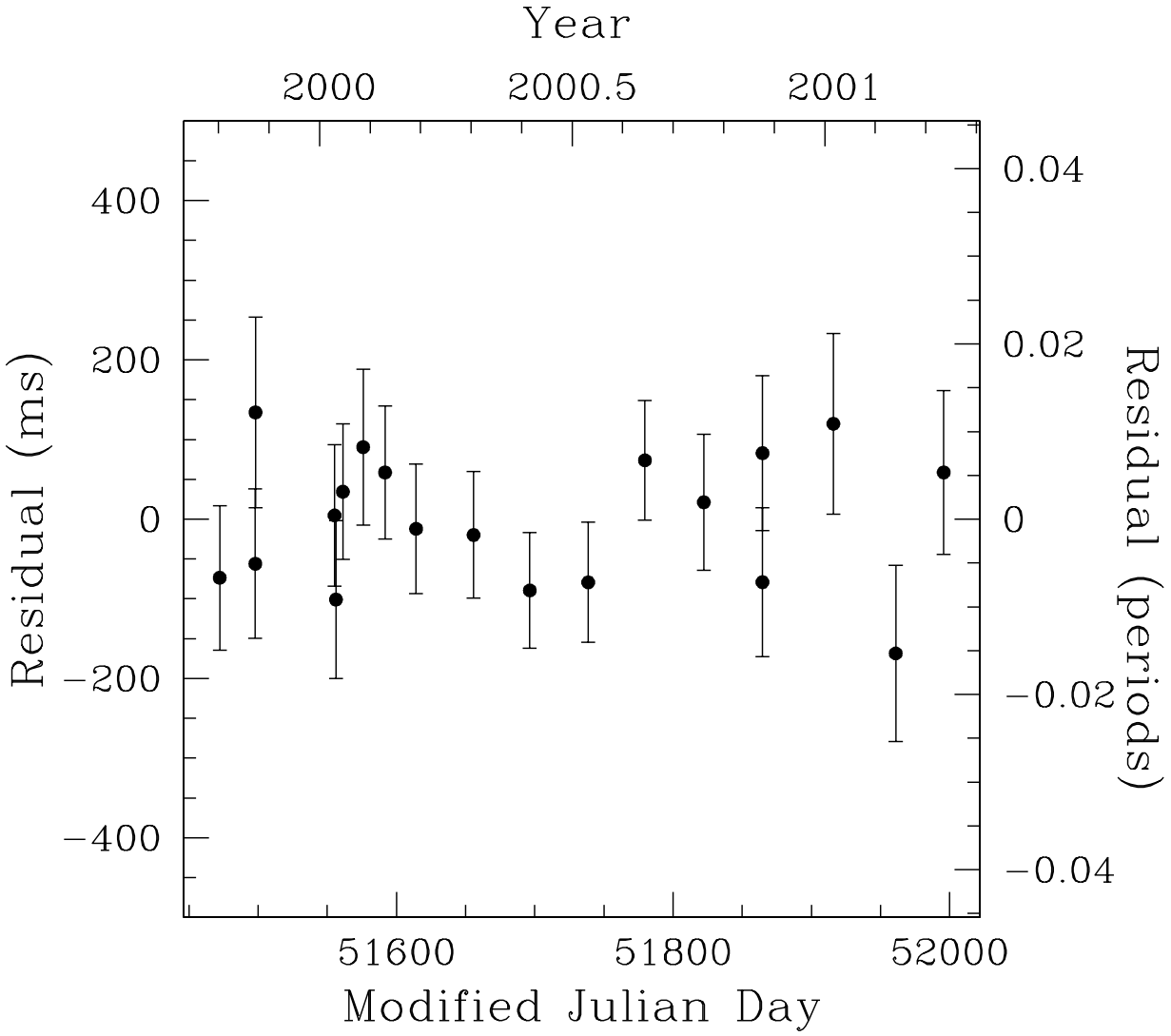

Fig. 5.— Arrival time residuals for 1RXS 1708–4009 with ν, $\dot{\nu}$ and $\ddot{\nu}$ subtracted.

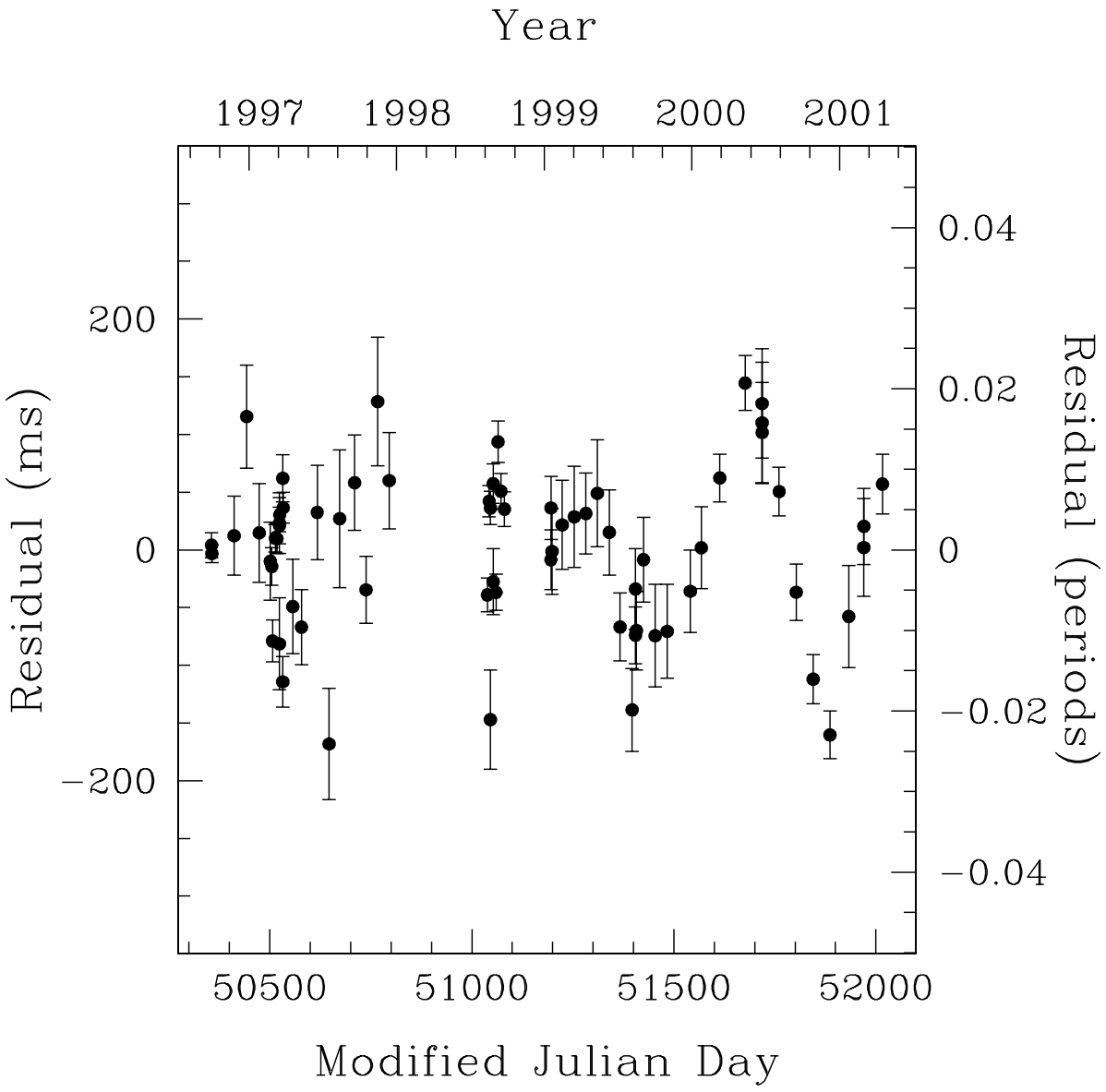

Fig. 6.— Arrival time residuals for 1E 2259.1+586 with ν, $\dot{\nu}$ and $\ddot{\nu}$ subtracted.

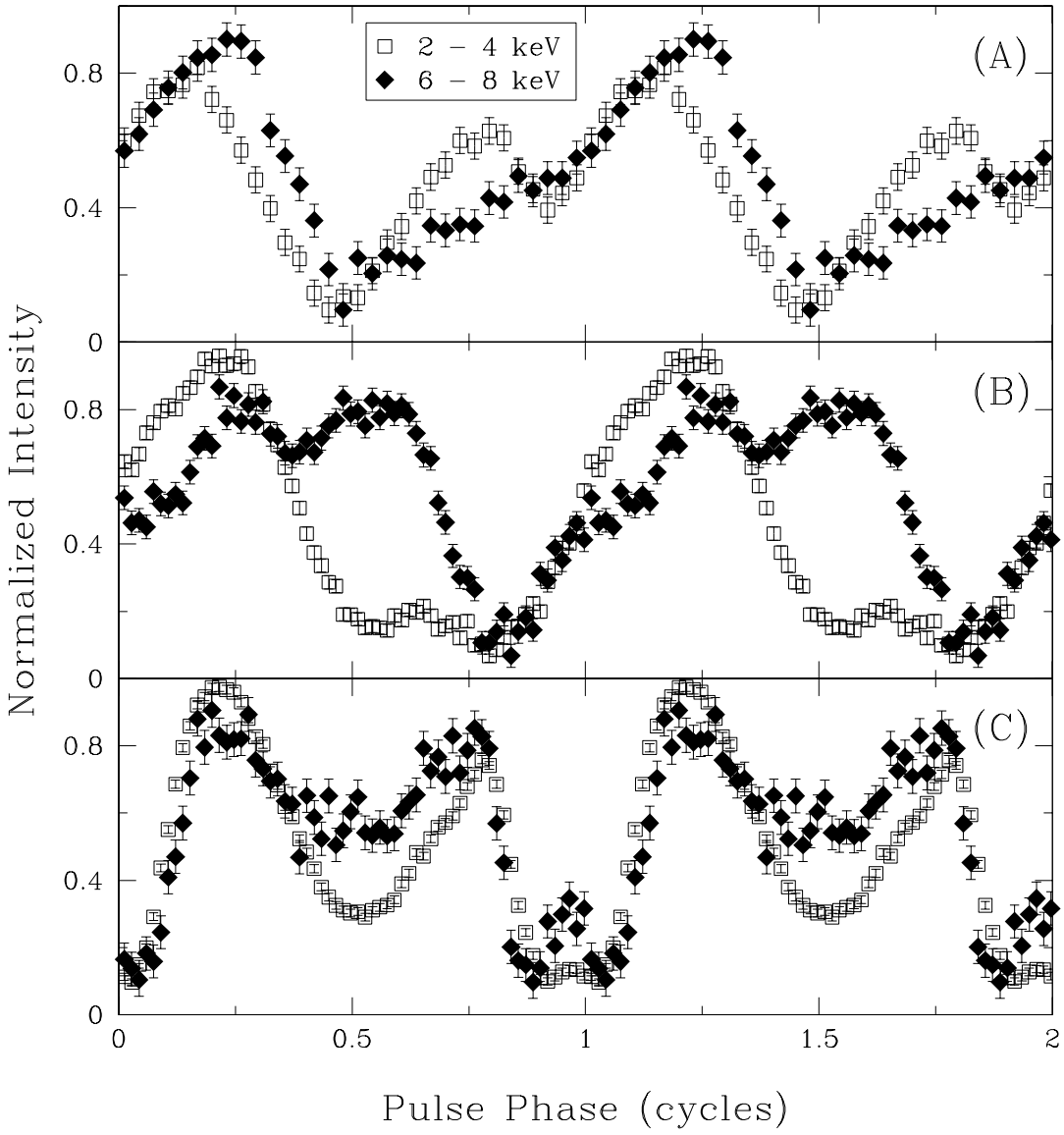

Fig. 7.— Average pulse profile of (A) 4U 0142+61, (B) 1RXS 1708–4009 and (C) 1E 2259.1+586 in two energy bands as observed by *RXTE*. Two cycles are plotted for clarity. Note that the scaling was chosen to minimize the χ^2 of the difference between the two profiles. Thus the only information that these plots convey is the relative amplitudes of the features of the profile.

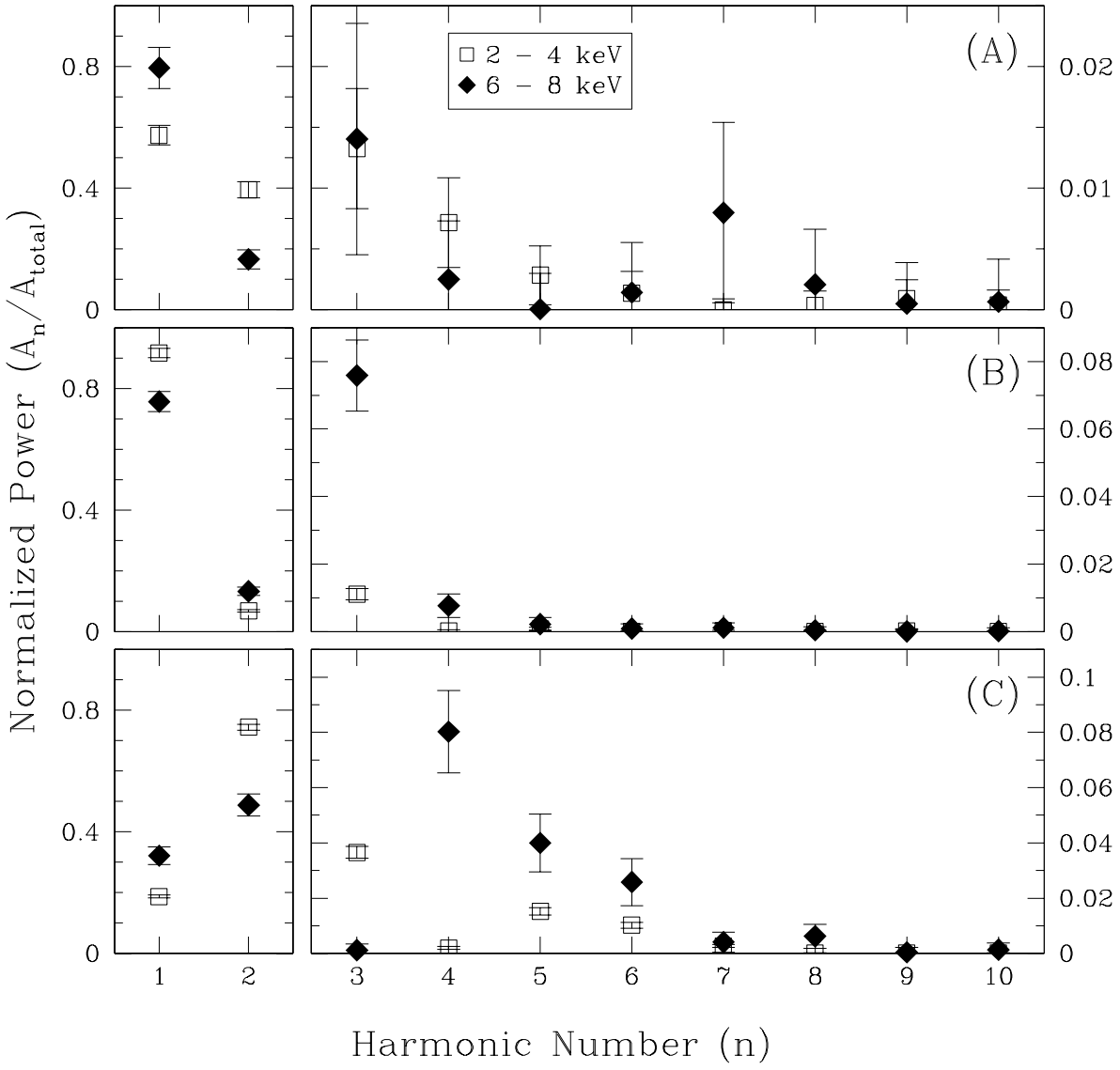

Fig. 8.— Harmonic content of the average pulse profiles in Figure 7 in three energy bands. (A) 4U 0142+61; (B) 1RXS 1708–4009; (C) 1E 2259.1+586. The ratio of the power in the $n^{\rm th}$ harmonic to the total power in all harmonics is plotted versus n.

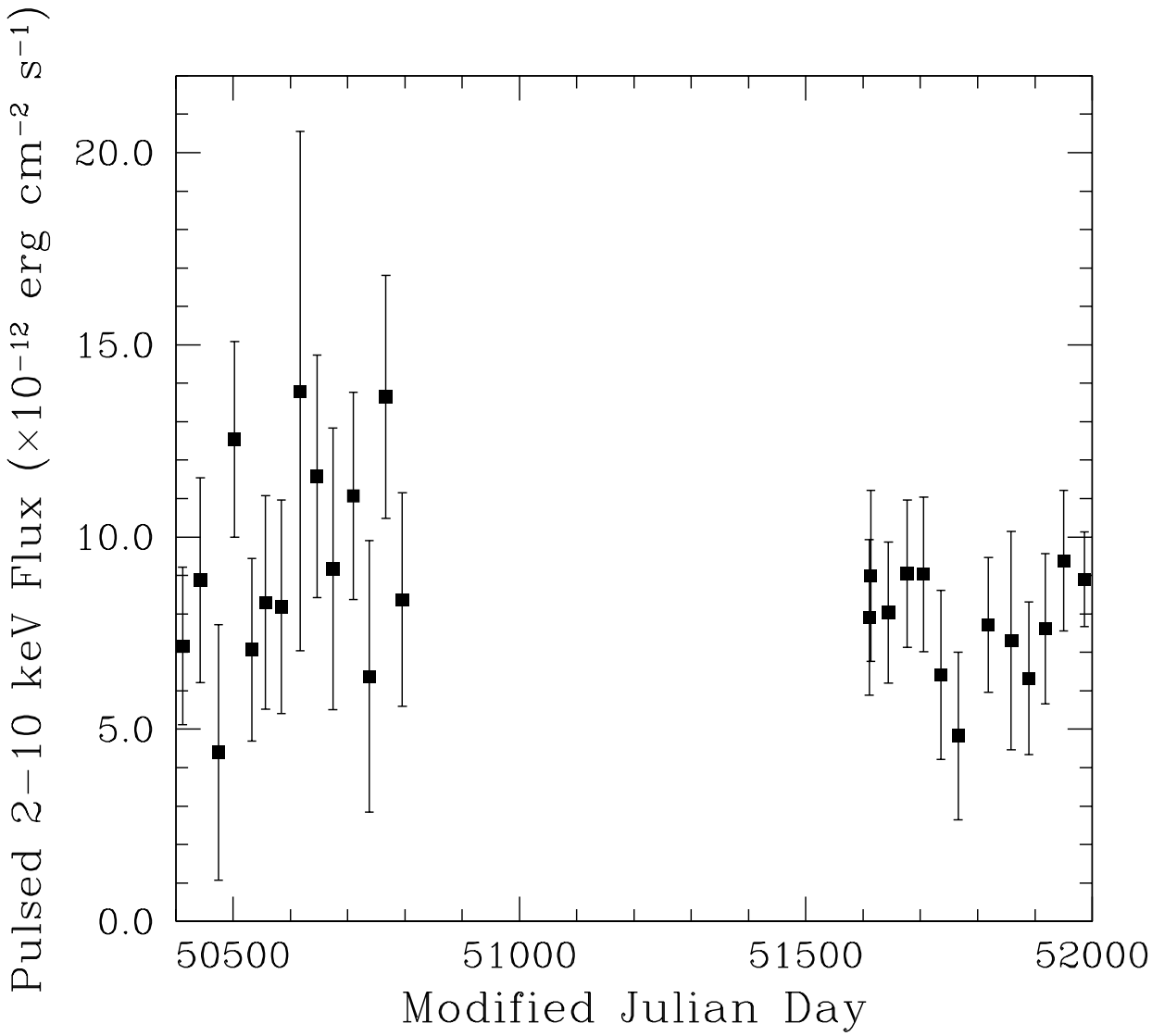

Fig. 9.— Pulsed flux time series for *RXTE* observations of 4U 0142+61. Error bars represent 1σ confidence intervals. See §3.4 for details of the analysis procedure.

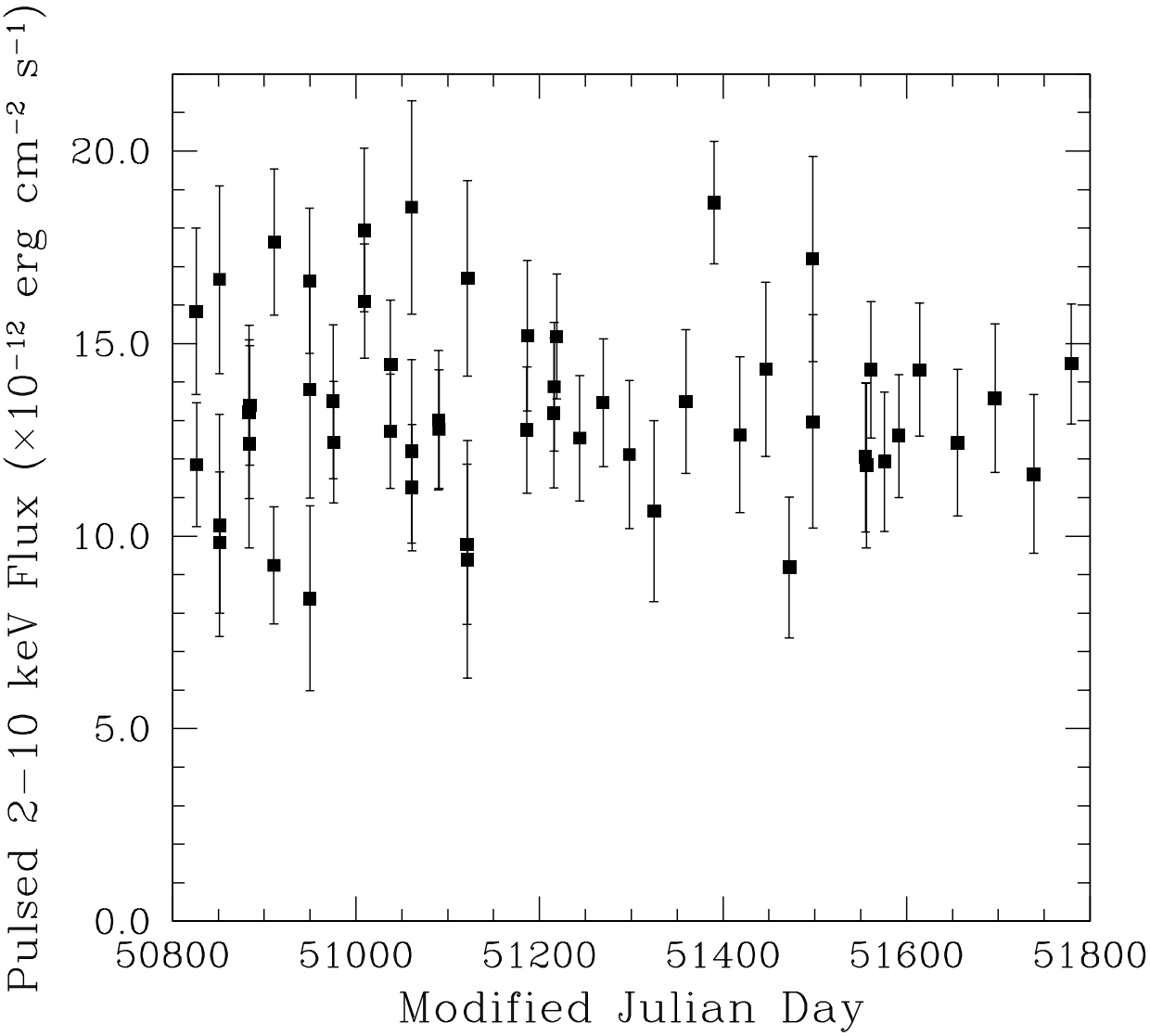

Fig. 10.— Pulsed flux time series for *RXTE* observations of 1RXS 1708–4009. Error bars represent 1σ confidence intervals. See §3.4 for details of the analysis procedure.

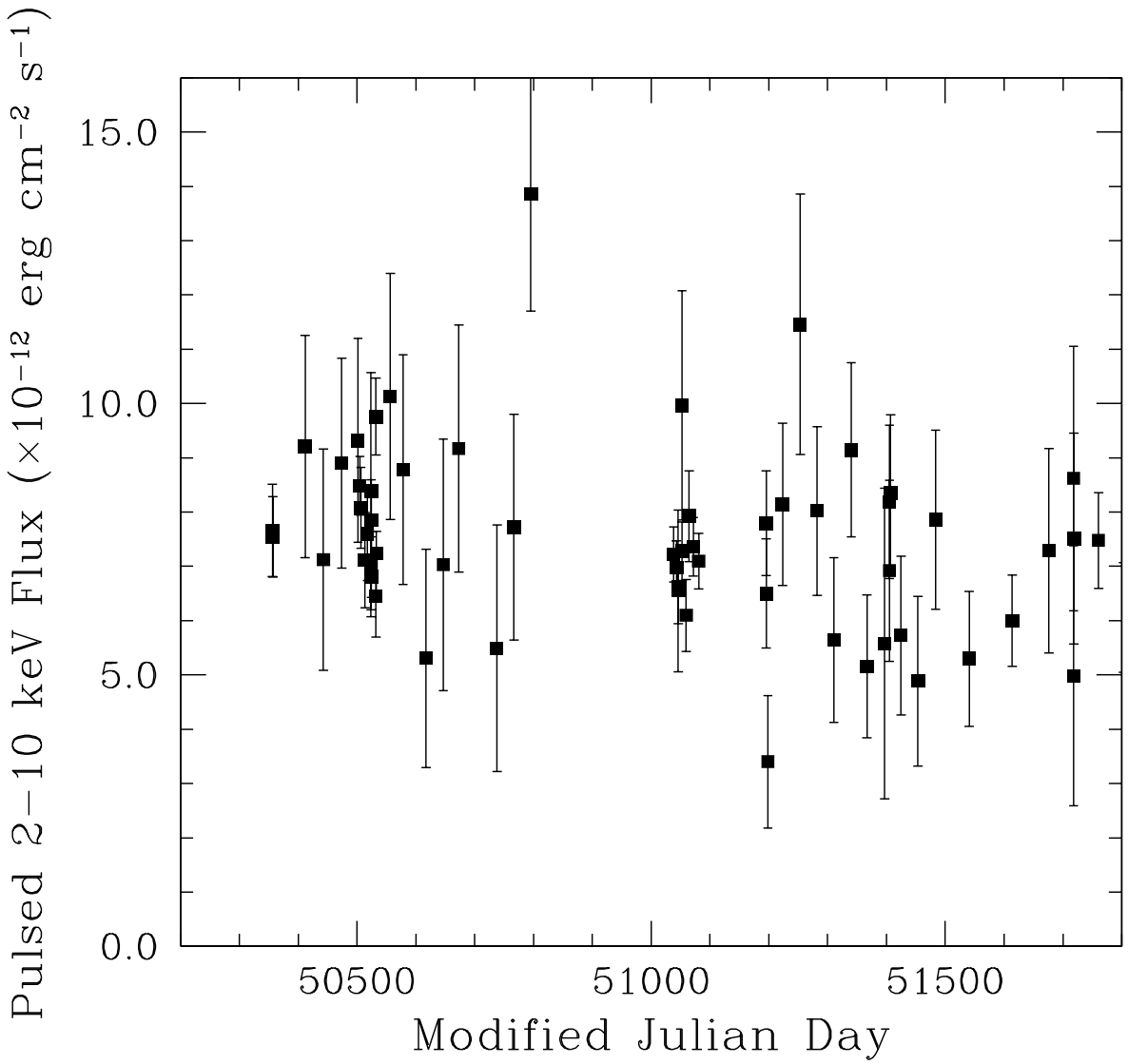

Fig. 11.— Pulsed flux time series for *RXTE* observations of 1E 2259.1+586. Error bars represent 1σ confidence intervals. See §3.4 for details of the analysis procedure.